ACS OMEGA

Open Access

This article is licensed under CC-BY-NC-ND 4.0

http://pubs.acs.org/journal/acsodf

Article

High-Performing Unitized Regenerative Fuel Cell Using PGM-Free Bifunctional Catalysts from Waste-Derived Carbon

Eva Sousa,◆ Sofia Delgado,◆ Fátima Santos, and Adélio Mendes*

Cite This: *ACS Omega* 2026, 11, 61767−61780

Read Online

ACCESS | Metrics & More | Article Recommendations | Supporting Information

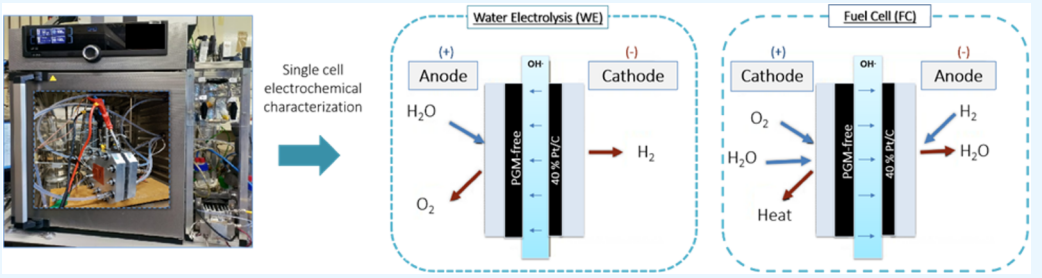

ABSTRACT: Unitized regenerative alkaline-exchange membrane fuel cells (UR-AEMFCs) are a promising technology for energy storage, attending to their ability to operate in both galvanic (FC) and electrolytic (WE) modes. However, their round-trip efficiency (RTE) is greatly dependent on the selected electrodes toward the oxygen reduction reaction (ORR) and oxygen evolution reaction (OER). As both mechanisms have slow kinetics, developing innovative and efficient bifunctional catalysts is critical to increasing UR-AEMFC performance. In this work, bifunctional precious group metal-free (PGM-free) catalysts were prepared by nucleating either Fe, Ni, or FeNi on nitrogen-doped carbons; the prepared catalysts have a maximum metal loading of up to 3 wt %. To align with circular economy principles, a sustainable approach was employed by using a phenolic resin-based waste product as a carbon precursor. The carbonization process, conducted in the presence of H_3PO_4 and melamine, yielded nitrogen-doped carbon supports with enhanced properties. Notably, in single-cell operation, the prepared PGM-free catalysts—NiNC, FeNC, and FeNiNC—generated RTEs of 29%, 38%, and 35%, respectively, under corrosion-free alkaline electrolytes (0.5 M KOH); similar results were reported for benchmark commercial catalysts such as IrO_2, which displayed *ca.* 30% of RTE. Moreover, NiNC catalyst showed a half-wave potential of 0.74 V, an onset potential of 0.88 V, and an overpotential of 420 mV at 10 mA cm^{-2}. In turn, the FeNC displayed a half-wave potential of 0.72 V, an onset potential of 0.90 V, and an overpotential of 510 mV at 10 mA cm^{-2}. Regarding the FeNiNC, this catalyst demonstrates a half-wave potential of 0.76 V, an onset potential of 0.86 V, and an overpotential of 380 mV at 10 mA cm^{-2}. These results are particularly noteworthy considering the significantly lower metal loadings in the produced PGM-free catalysts. Besides, to evaluate their long-term performance, the single cell was submitted to several potential cycles within the potential window range for FC and WE modes, i.e., between 0.6 and 2.0 V. The noble Pt/C catalysts deactivated completely after the stress test, while the novel FeNiNC and NiNC catalysts, containing an ultralow loading of critical raw materials (CRMs), demonstrated an outstanding compromise between activity and stability, proving their potential to be integrated in UR-AEMFC.

1. INTRODUCTION

The energy storage panorama is continuously evolving, owing to the rising demand for portable devices and due to the urgency of effectively incorporating renewable energy sources. Batteries are the most often used devices for storing energy easily and efficiently interconvertible in electricity; nonetheless, batteries are not appropriate for long-term operation due to their self-discharge.[1] Particularly, many applications rely on Li-ion batteries, but their manufacturing processes involve the use of highly flammable organic electrolytes, which have a severe negative influence on their disposal after use. Furthermore, lithium extraction has been a topic of concern due to its strong environmental impact.[2] Therefore, other technologies have gained traction alongside batteries in recent years. For instance, unitized regenerative fuel cells (URFCs) have been considered a promising technology for energy storage due to their compact configuration, light overall weight, ability to produce clean energy, and high specific energy density.[3] Their dual function as fuel cell (FC) and electrolyzer (WE) makes them a suitable choice, particularly as an on-site energy storage system, such as for integration into residential/corporative buildings. Nevertheless, their round-trip efficiency (RTE),

Received: June 29, 2026
Revised: September 14, 2026
Accepted: September 17, 2026
Published: September 30, 2026



ACS Publications

© 2026 The Authors. Published by American Chemical Society

https://doi.org/10.1021/acsomega.6c07541
ACS Omega 2026, 11, 61767−61780

Downloaded from pubs.acs.org/acsodf/article-pdf/11/40/61767/6872059/acsomega.6c07541.pdf by UNIVERSIDADE DO PORTO 01100 user on 25 November 2026

meaning their effectiveness in storing and retrieving the stored energy, is still heavily reliant on the applied electrocatalysts toward oxygen-involving reactions due to their sluggish kinetics. In a URFC, each electrode should be bifunctional to sustain both modes of operation, which is highly challenging.[4] Besides, the dual function generates limitations regarding water and gas management at the porous transport media and catalyst layer level when switching from galvanic (FC) to electrolytic (WE) modes, which normally results in steep mass transport overpotentials.[5]

Particularly, unitized regenerative proton exchange membrane fuel cell (UR-PEMFC) is the most mature technology, but the high costs associated with the use of noble metal catalysts and the expensive non(bio)degradable perfluorosulfonic-based membranes used to boost ion exchange capacity (*i.e.*, Nafion) are hindering their large-scale commercialization.[6] In detail, Pt-based catalysts are known for their high catalytic activity toward oxygen reduction reaction (ORR), whereas IrO_2 is often considered the benchmark catalyst for oxygen evolution reaction (OER), given its superior stability and activity at higher potentials. Currently, some of the best UR-PEMFC systems reveal an overall maximum round-trip efficiency of 60% at moderate current densities of 0.4 A cm^{-2} in acidic media, though when employing highly prohibitive loadings of precious group metal (PGM) catalysts (Pt, Ru, Ir) of around 1−7 mg_{PGM} cm^{-2}.[7]

Due to the limited availability of platinum and iridium, those metals are designated as critical raw materials (CRMs).[8] In 2023, the EU elaborated the CRMs list, which comprises the raw materials with significant economic relevance for the European Union and high supply-related risk, with the latest updates including already battery-grade nickel and copper, among others.[9] The European Union is, therefore, increasingly concerned about having consistent and unrestricted access to these specific raw commodities, so it is important to note that it is now even more crucial to develop catalyst configurations and electrochemical systems that have low content or that are free of CRMs.

On the other hand, thanks to the major breakthroughs in the development of highly conductive stable anion exchange membranes (AEMs), ionomeric binders, and precious group metal (PGM)-free catalysts for oxygen-involving reactions in alkaline media, unitized regenerative AEM fuel cells (UR-AEMFC) have gained considerable attention in the recent years. The deployment of recent highly conductive yet cheaper anion exchange membranes for operation in low-concentration of KOH circulating electrolytes, namely quaternized ammonium/poly(arylene piperidinium, has allowed reaching peak power densities of *ca.* 2 W cm^{-2} in AEM fuel cells at moderate temperature and low pressure (0.1 MPa).[10] Similar polymeric formulations had been tested in AEM water electrolyzers and allowed to reach nearly 3.5 A cm^{-2} at 1.8 V and 60 °C.[11] Such advances may play a critical role in aligning innovative paths toward the construction of novel configurations of UR-AEMFC systems.

Moreover, PGM-free bifunctional catalysts made of 3d transition metals (Ni, Fe) are foreseen as the new generation of materials to feature low cost alongside high reversibility, activity, and stability toward OER/ORR, in the detriment of common Ir−Pt mixtures, especially under alkaline conditions.[12] The latter is relevant since the kinetics of both OER/ORR tend to be higher in alkaline environments.[13] Furthermore, normally, the costs with Pt or Pt alloy electrocatalysts for ORR are approximately 50 € g^{-1}. Ir-based oxides for OER are around 150 − 200 € g^{-1}. On the other hand, transition metals such as Fe (0.0001 € g^{-1}), Mn (0.02 € g^{-1}), and Ni (0.02 € g^{-1}), are significantly cheaper, thus, making the use of PGM-free catalysts an effective and essential solution also to decrease drastically the CAPEX associated with URFC devices.[14]

Still, Ni-based electrodes with large loadings for AEM applications remain preponderant for achieving interesting OER efficiencies, which is a concern given the latest lists of CRMs. Nonetheless, early studies reported that, typically, $Ni(OH)_2$ activity toward oxygen evolution can be highly enhanced by incorporating Fe, even when iron is added at ultralow concentrations.[15] In fact, NiFe-based nanoparticles comprising alloys, oxides, and NiFe-layered double hydroxides (NiFe-LDHs) have been considered excellent OER electrocatalysts in alkaline media. Different strategies have been employed to improve their performances, including the size and morphology optimization, introduction of defects and vacancies to adjust intrinsic electronic structures, and their dispersion over high surface area substrates, such as carbon to enhance conductivity and provide improved mass transport pathways.[16]

Among recent discoveries, nitrogen-coordinated Fe atoms dispersed over carbon-based supports (FeNC) have spiked special attention toward oxygen reduction in alkaline media, revealing relevant catalytic activities. Interestingly, FeNC catalysts are normally carbonaceous materials with many phases containing small amounts of metal, <5 wt %.[17] Most authors claim that Fe-Nx-based species with pyridinic-N coordination have an optimal synergetic effect, which has been ascribed to improve its electroactivity.[18] Although the pyridinic N species have been demonstrated to be advantageous for ORR processes over a wide pH range, there is still controversy regarding the catalytic mechanisms and the role of N species on the performance of nitrogen-doped-based catalysts. The findings of Lin Y. et al. indicate that pyridinic N species are prone to contribute to a four-electron-transfer mechanism toward oxygen reaction, and their presence improves the onset potential of ORR.[19] Their simulations showed that pyridinic N can also accelerate efficiently the OER process. Those effects were ascribed to an enhanced electron delocalization effect from a larger π-conjugated system; in fact, for the authors, the structure size of π-conjugated pyridinic N species is seen as the critical factor in facilitating OER/ORR processes. Hence, continuous efforts are being pursued to maximize the utilization of such active species while boosting the surface area of the supports.[20]

Thereupon, doping high-surface and conductive materials with 3d transition metals emerges as a promising alternative to PGM catalysts to ensure higher OER/ORR catalytic activities. The mentioned breakthroughs rule the motivation of this work, which consisted of the development of bifunctional structures of metal (Fe, Ni) nucleated on nitrogen-doped carbon for OER/ORR and their subsequent assessment in a UR-AEMFC. Within the context of sustainability and circular economy, carbon recovery from waste products is an essential research topic, where derived carbon-based nanomaterials may find multiple new applications in the landscape of energy conversion and/or storage. Therefore, in this work, waste of phenolic resins served as the source to produce nitrogen-doped carbon supports.

Downloaded from pubs.acs.org/acsodf/article-pdf/11/40/61767/6872059/acsomega.6c07541.pdf by UNIVERSIDADE DO PORTO 01100 user on 25 November 2026

https://doi.org/10.1021/acsomega.6c07541
ACS Omega 2026, 11, 61767−61780

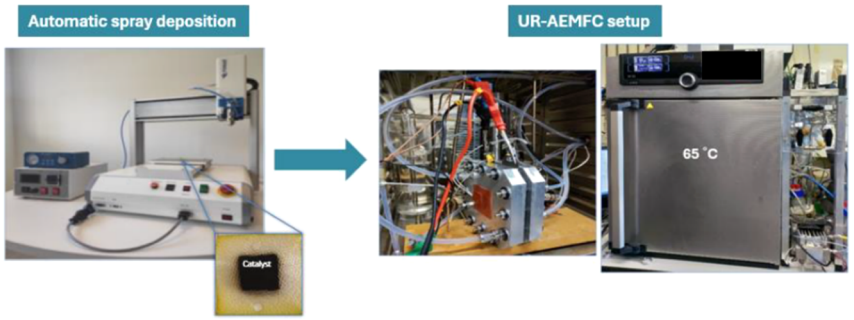

Figure 1. Catalyst layer preparation via spray deposition and experimental UR-AEMFC test bench.

In detail, the produced PGM-free based electrodes, consisting of synthesized FeNC, NiNC, and FeNiNC yielded great current densities both in galvanic and electrolytic modes and an interesting bargain between round-trip efficiency and stability in comparison to commercial 40 wt % Pt/C and IrO_2, also considering the operation under much less corrosive conditions (*i.e.*, 0.5 M KOH) than usual − higher than 1 M KOH. In this study, the prepared UR-AEMFCs with PGM-free oxygen electrodes made of FeNC, NiNC, and FeNiNC, containing ultralow loading of metal <3 wt %, attained significant efficiencies of 38%, 29%, and 35%, respectively, at 30 mA cm^{-2}, which is a promising result knowing the average RTE of mature UR-PEMFC systems is usually between 35% and 55%.[21−23] These novel catalysts proved to provide an adequate balance between activity and stability, even with only an ultralow metal loading. Following these findings, the proposed sustainable and less expensive methods of producing bifunctional electrodes and, ultimately, unitized regenerative fuel cells, may be highly strategic and effective solutions to develop promising devices.

2. EXPERIMENTAL SECTION

2.1. Synthesis of PGM-Free Catalysts

Fe, Ni, and FeNi nanoparticles were nucleated over nitrogen-doped carbon supports. In detail, a residue of phenolic resin-based powder (from floral foam) was used as a carbon source to produce N-doped supports. Before the carbonization step, which occurred at 1000 °C under nitrogen, the phenolic resin-based powder was mixed with melamine (Alfa Aesar) considering a mass ratio of 1:1; the mixture was stirred overnight in the presence of H_3PO_4 (3:1 acid/powder mass ratio). This initial carbonization at 1000 °C under nitrogen allowed to convert the phenolic-resin-derived precursor into a highly carbonized and N-doped carbon support.

Afterward, PGM-free catalysts were prepared by dispersing 1 g of melamine in a small volume (20 mL) of ultrapure water at 80 °C, followed by adding a sample of 18 mg of metal salt precursor to the solution. FeNC, FeNiNC, and NiNC catalysts were produced by mixing $Fe(NO_3)_3{\cdot}9H_2O$ (Sigma-Aldrich) and/or $Ni(NO_3)_2{\cdot}6H_2O$ (Sigma-Aldrich) as metal salt precursors. For the synthesis of bimetallic FeNiNC, Fe- and Ni- precursors were dissolved using a molar proportion of 1:1. Finally, 100 mg of the previously made H_3PO_4-activated carbon support was further added to the solution, which in turn was stirred at 120 °C until all water was evaporated. Then, produced nanoparticles were collected and subjected to a thermal treatment under argon at 550 °C for 3 h and, subsequently, heated up to 750 °C for 1 h. The first thermal treatment at 550 °C allowed to decompose the metal nitrate precursors and promote the initial formation and dispersion of the metal-containing species within the N-doped carbon matrix. Then, the second thermal treatment at 750 °C stabilized the metal-containing nanoparticles and their interaction with the carbon support, at the same time that avoided more severe structural changes that could be observed under 1000 °C.

The performance of the as-prepared non-noble catalysts was compared to the results achieved by a catalyst supported on nitrogen-doped carbon using commercial Ketjenblack EC-600J (Tanaka) as a carbon source, which was denoted as FeNiNC/Ketjenblack. Also, commercially available Ni/C (Premetek), Pt/C (Premetek), and IrO_2 (Sigma-Aldrich) were used as benchmark catalysts.

2.2. Morphological Characterization

The prepared PGM-free catalysts were subjected to Inductively Coupled Plasma−Optical Emission Spectroscopy (ICP-OES; Thermo iCAP 7000) to obtain Fe and Ni mass fractions. For that, a sample of 10 mg of each catalyst was dissolved in 10 mL of *aqua regia* at 100 °C. Besides, a thermogravimetric analyzer (TG 209 F1 iris, NETZSCH) was used to assess the thermal behavior of the non-noble catalysts under an oxidative environment (O_2), with heating ranging from 25 to 900 °C.

The surface area and porosity of the prepared catalysts were analyzed by performing nitrogen isotherms at 77 K (Quantachrome Autosorb-1 Instruments). Before analysis, all samples were thoroughly degassed under vacuum at 200 °C for 4 h.

Transmission electron microscopy (TEM; Jeol 2200FS) was utilized to examine the morphology of the prepared catalysts and the dispersion of Fe and Ni over the supports. The samples for TEM were prepared by dispersing a small quantity of powder in ethanol, and a small aliquot was subsequently deposited on a copper grid.

Surface composition and chemical interactions between elements were evaluated using X-ray photoelectron spectroscopy (XPS). XPS spectra were acquired using an ESCALAB 250Xi (Thermo Fisher Scientific) with base pressure below 5×10^{-10} mbar. The system has a hemispherical electron energy analyzer with an energy resolution 0.1 eV, and a monochromated X-ray source. The spectra were recorded at the pass energies 100 and 40 eV for the survey spectra and individual elements, respectively. XPS spectra were analyzed using CasaXPS software. In XPS analysis was used a Shirley background subtraction method, a carbon C 1s = 284.8 eV as reference for conductive carbon materials, and a mixed Gaussian−Lorentzian line shapes with peak fitting constraints on the peak position and peak area,

The crystal structure and nature of crystalline phases were investigated by X-ray diffraction (XRD; Bruker AXS Smart APEX) analysis. The X-ray patterns were obtained using Cu Kα radiation at Cu Kα1 = 1.5406 Å) over the range 15−80°.

2.3. Electrochemical Characterization in RDE and Single Cell

The electrochemical characterization of PGM-free catalysts was performed in a rotating disk electrode (RDE) comprising a gold (Au) disk as the working electrode, a carbon rod as an electron donor serving as counter electrode, and a solution of Ag/AgCl in 3 M KCl(aq) as the reference electrode. The catalyst ink was prepared by ultrasonically dispersing 5 mg of catalyst in 125 μL of isopropanol (VWR), 560 μL of ultrapure water, and 54 μL of Sustainion ionomer (Dioxide Materials, 5 wt %). Subsequently, a sample of 10 μL (*ca.* 400

Downloaded from pubs.acs.org/acsodf/article-pdf/11/40/61767/6872059/acsomega.6c07541.pdf by UNIVERSIDADE DO PORTO 01100 user on 25 November 2026

https://doi.org/10.1021/acsomega.6c07541
ACS Omega 2026, 11, 61767−61780

μg cm^{-2} for the prepared PGM-free catalysts) was deposited over the Au disk and left to dry at 700 rpm.

The bifunctionality of the prepared catalysts was assessed by performing linear sweep voltammograms (LSVs) in oxygen-saturated 0.1 M KOH electrolyte at 25 °C. LSVs were obtained by scanning the potential of the Au disk from 0.05 to 2.5 V (vs reversible hydrogen electrode [RHE]) at 20 mV s^{-1} with a rotation rate of 1600 rpm. For assessing the stability of the manufactured catalysts, a stability protocol was applied by cycling the potential of the working electrode in the potential range between 0.6 V and 2 V for 3000 cycles at 500 mV s^{-1}.

The prepared catalysts were further applied in a UR-AEMFC (Figures 1 and 2). Carbon cloth (Fuel Cell Store) was utilized as the

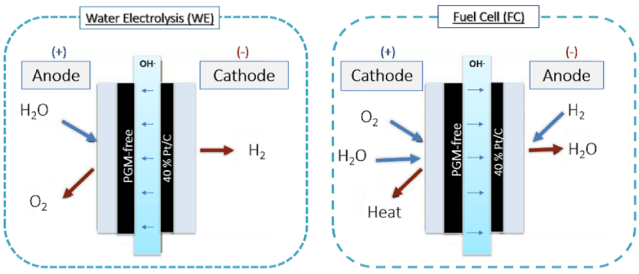

Figure 2. Sketch of the two working modes.

reactants' diffusion layer and, thereby, as the substrate for depositing the catalysts. Before deposition, a sample of carbon cloth was immersed in 1 M HNO_3 (VWR) for 3 h at 80 °C. Then, oxygen bifunctional catalyst layers were prepared via spray deposition of the catalyst suspension, which in turn was prepared by dispersing the catalyst powder in a 1:1 (v/v) volume ratio of water/isopropanol containing 25 wt % Sustainion ionomer (dioxide materials, 5 wt %). PGM-free catalyst loading onto the carbon cloth was set to 3 mg cm^{-2} (loading of metals was 90 μg cm^{-2}, ca. 3 wt %), whereas a commercial 40 wt % Pt/C (0.3 mg cm^{-2}, Premetek) was used in the opposite electrode. The loading of Pt/C and IrO_2 in the prepared benchmark catalyst layers was set to 1 mg cm^{-2}. This difference may influence catalyst-layer thickness, porosity, ionic resistance, and mass-transport behavior, among others. Therefore, this limitation must be considered in the following sections, when the absolute power densities of the different catalyst systems are compared. Moreover, the single-cell results must be interpreted to compare the evolution of the catalyst layers under the tested conditions, instead of a direct measurement of their intrinsic activity.

A sustainion membrane (dioxide materials) was activated overnight in 0.1 M KOH before being used as a solid polymeric electrolyte to separate both electrodes. The electrodes were assembled in a Pragma cell (6.25 cm^2 active area) using graphitic flow fields engraved with serpentine-shaped channels. When operating in fuel cell mode (FC), the reactants—hydrogen, and oxygen (50 mL min^{-1} and 300 mL min^{-1}, respectively)—were fed to the system at 65 °C and 1 bar under fully humidified conditions. Under electrolyzer mode (WE), a constant flow of 0.5 M KOH was fed to the anodic compartment at 65 °C.

The electrochemical characterization of the single-cell configuration was carried out using an AutoLab PGSTAT with Booster 10 A. Polarization curves were recorded between 0.05 and 2.0 V at 10 mV s^{-1}. Electrochemical impedance spectroscopy (EIS) was executed in potentiostatic mode between 50 mHz − 15 kHz at 0.5 V with an amplitude perturbation of 10 mV, and in galvanostatic mode at 200 mA cm^{-2}, perturbation of 100 mA. A stability assessment of catalysts was performed by cycling the potential of the system between 0.6 to 2.0 V for 8000 s at a scan rate of 5 mV s^{-1}.

3. RESULTS AND DISCUSSION

3.1. Oxygen Bifunctional Catalysts Morphological Characterization

In this study, phenolic resin-derived N-doped carbon supports were prepared via carbonization (at 1000 °C under nitrogen) of residues of floral foam in the presence of H_3PO_4, which was used as an activating agent. Although the precise chemical mechanism of H_3PO_4 activation during pyrolysis is still unclear, some authors have reported that H_3PO_4 preferentially reacts with the surface oxygenated groups, which in turn is seen as beneficial to enhance the specific surface area and optimize the pore size distribution of the final carbonaceous structure.[24] Engineering an appropriate catalyst surface is critical to ensure performance-determinant features such as corrosion-resistance, conductivity, high surface area, and accessibility.

First, the morphology of the prepared catalysts was evaluated through TEM analysis, which clearly showed Fe and Ni nanoparticles nucleated over nitrogen-doped carbon (Figure 3). The metallic nanoparticles are mostly spherical and

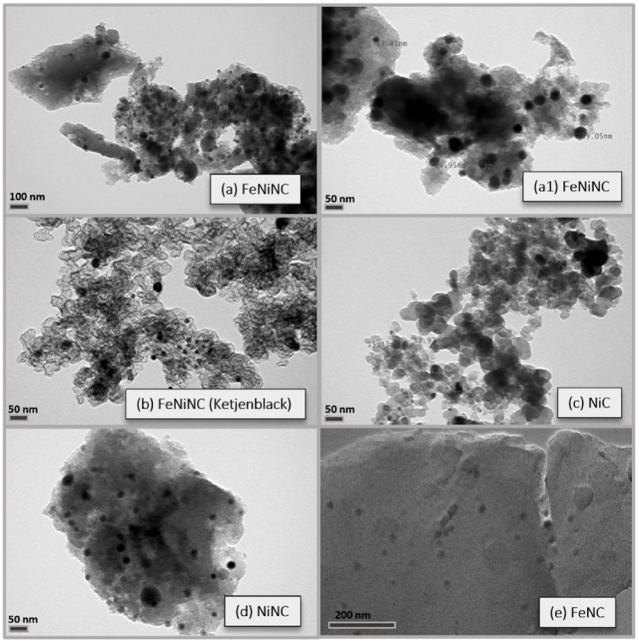

Figure 3. TEM images of: FeNiNC at 100 000× (a) and 200 000× (**a1**), respectively; FeNi-based catalyst supported on nitrogen-doped Ketjenblack at 200 000× (b); commercial Ni/C at 200 000× (c); NiNC at 200 000× (d); FeNC at 40 000× (e).

well dispersed over the carbon support. Table S1 provides a summary of the average size of the produced nanoparticles. While the manufactured FeNiNC and FeNiNC/Ketjenblack exhibit greater metallic sizes of *ca.* 22.84 ± 7.22 nm and 18.46 ± 6.81 nm (Figure 3a and Figure 3b), respectively, the commercial Ni/C sample (Figure 3c) exhibits a smaller Ni particle size of 12.37 ± 4.73 nm, which is closer to the sizes of the NiNC sample (Figure 3d), −13.91 ± 4.47 nm.

Overall, the FeNiNC catalyst reveals larger and intermetallic Fe and Ni nanoparticles. Besides, the phenolic resin-derived carbon particles reveal a dense carbonaceous layer,[25] while the catalysts supported on Ketjenblack (Figure 3b) show an irregular surface texture, which is typical of more amorphous carbons.[26]

Downloaded from pubs.acs.org/acsodf/article-pdf/11/40/61767/6872059/acsomega.6c07541.pdf by UNIVERSIDADE DO PORTO 01100 user on 25 November 2026

https://doi.org/10.1021/acsomega.6c07541
ACS Omega 2026, 11, 61767−61780

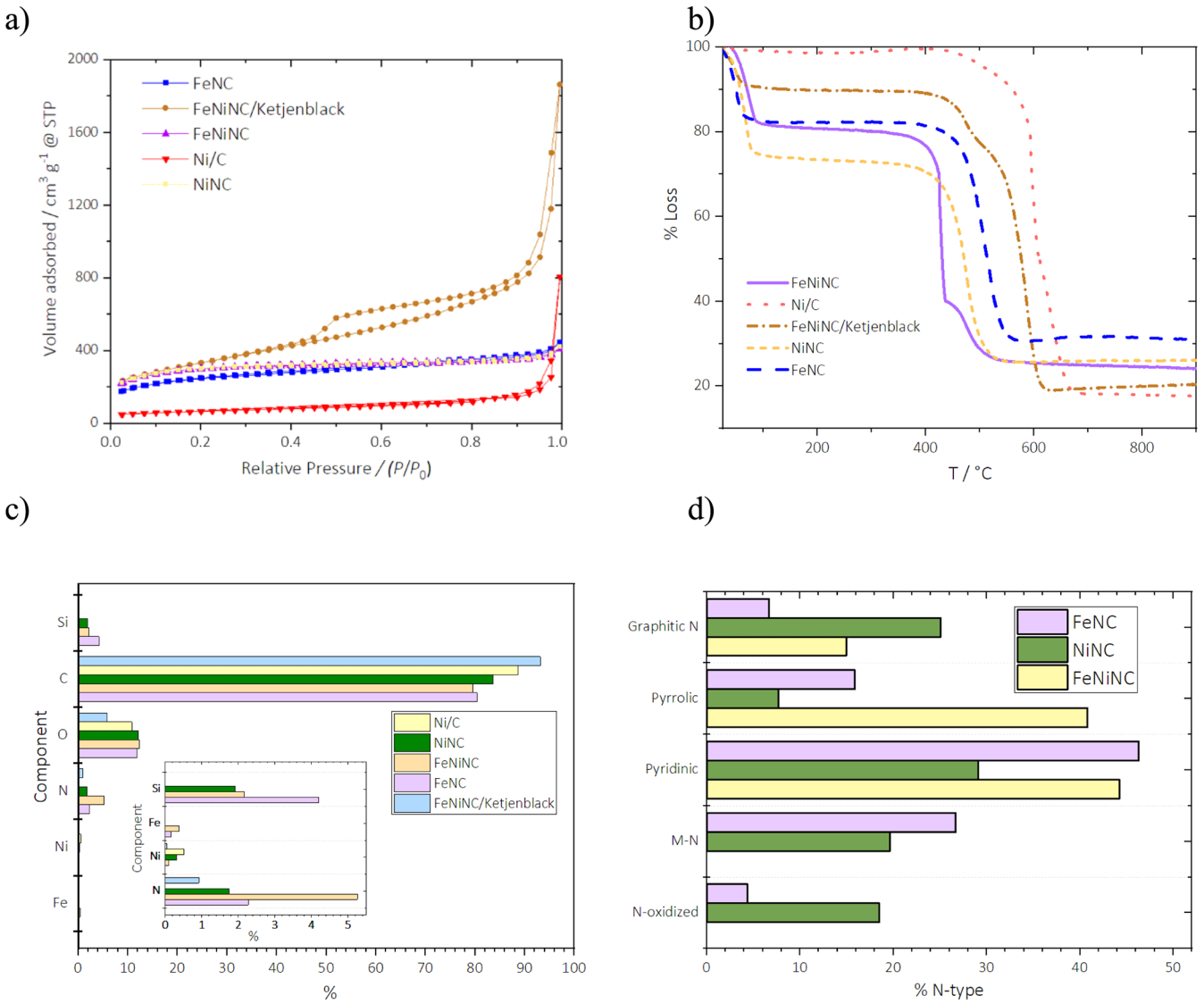

Figure 4. N-isotherms of the prepared PGM-free catalysts comparison with commercial Ni/C (a); thermogravimetric behavior of catalysts under oxygen up to 850 °C (b); atomic concentration of each component from XPS (c); nitrogen-type concentration on the prepared FeNC, NiNC, and FeNiNC catalysts (d).

Figure 4a exhibits the nitrogen adsorption isotherms of the prepared catalysts at 77 K. FeNiNC/Ketjenblack shows a Type III hysteresis loop isotherm, which is characteristic of mesoporous materials with capillary condensation, whereas Ni/C revealed a higher concentration of macropores, as nitrogen adsorption only increases for higher relative pressures. The prepared PGM-free catalysts supported on H_3PO_4-activated N-doped carbons displayed a considerably higher N_2 uptake over a wide range of relative pressures, which indicates the development of a highly porous carbon structure.[27] In fact, FeNiNC/Ketjenblack, FeNiNC, NiNC, and FeNC catalysts reached great surface areas of 1184.6 m^2 g^{-1}, 961.0 m^2 g^{-1}, 954.7 m^2 g^{-1}, and 814.5 m^2 g^{-1}, respectively, whereas commercial Ni/C has a much lower surface area of 227.6 m^2 g^{-1}. So, the prepared PGM-free catalysts possessed approximately 3.6−5.2 times higher specific surface areas than Ni/C, which provides a larger interface for the electrolyte and the gaseous reactants to interact with the catalyst surface. The apparent multilayered architecture displayed by the prepared non-noble catalysts can be ideal for ensuring higher catalytic OER/ORR performances. The limited confined environment at micropores usually results in the retention of a larger concentration of reaction intermediates, which may then easily interact with the local surroundings. This factor may be critical during the synthesis process to guarantee the stronger retention of metal-active nanoparticles hosted near micropores. Also, this higher proximity of active sites to the carbon walls in microporous structures can generate efficient electron transfer pathways, allowing an increased ORR/OER activity. On the other hand, the mesoporosity ensures proper accessibility of reactants to those active sites.[28]

The thermal response of the produced catalysts under oxygen flow up to 900 °C is shown in Figure 4b. According to the thermogravimetric study, the synthesized phenolic resin-derived carbon-supported PGM-free catalysts exhibit a much larger mass loss at dehydration temperature (100 °C). The increased adsorption and retention of water molecules within the manufactured carbon structures may be caused by their microporosity.[29] Furthermore, the significant mass loss observed between 400 and 600 °C was attributed to carbon

Downloaded from pubs.acs.org/acsodf/article-pdf/11/40/61767/6872059/acsomega.6c07541.pdf by UNIVERSIDADE DO PORTO 01100 user on 25 November 2026

https://doi.org/10.1021/acsomega.6c07541
ACS Omega 2026, 11, 61767−61780

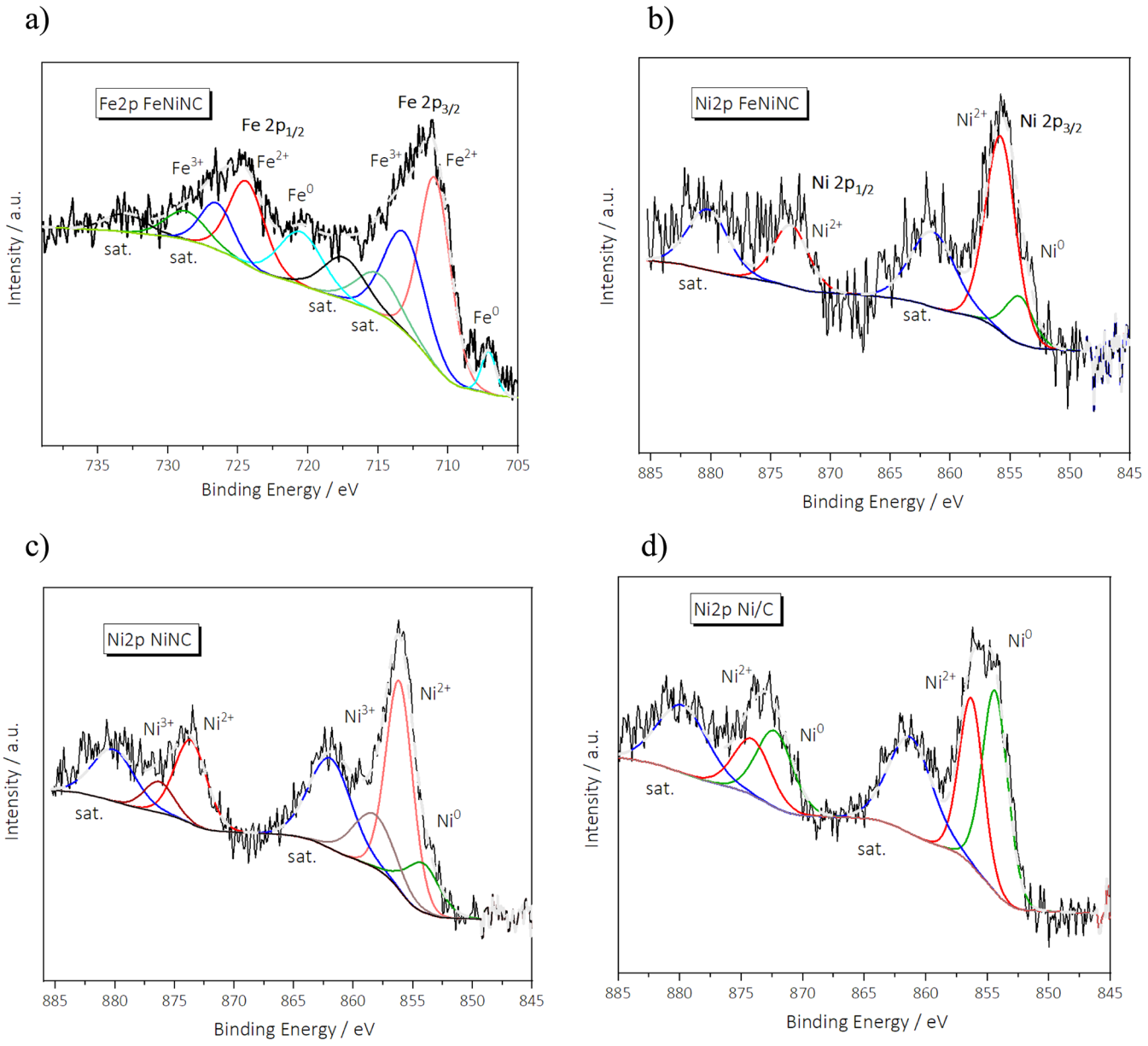

Figure 5. Deconvolution of Fe 2p orbital of FeNiNC (a), and Ni 2p of FeNiNC (b), NiNC (c), and Ni/C catalysts (**d**).

decomposition. Carbon stability appears to be higher under an oxidized environment for FeNiNC/Ketjenblack and Ni/C since their mass loss occurs at higher temperatures. Still, it is worth noting that high loadings of metal nanoparticles (Fe/Ni) on N-doped carbon supports can accelerate catalyst degradation at elevated temperatures due to direct thermal reactions between the metal and the support. The apparent lower thermal stability of the phenolic resin-derived carbon supports might be attributed to the higher concentration of metal nanoparticles and nitrogen functionalities within their structure.[30]

Figure 5a depicts the XPS spectra of the PGM-free catalysts, and Figure 4c reveals their chemical composition, namely, the atomic concentration of C, N, O, Fe, Ni, and Si present in the samples. The atomic fractions of Ni and Fe at the near-surface of FeNiNC (0.39 at. % and 0.11 at. %, respectively) are indeed slightly greater than the values obtained for FeNiNC/Ketjenblack (*ca.* 0.10 at. %). Even according to ICP data, the bulk mass fractions of Fe and Ni in FeNiNC are 1.01 and 1.81 wt %, respectively, while the mass fractions of both elements in FeNiNC/Ketjenblack are 0.97 wt % Fe and 1.69 wt % Ni. Besides, NiNC and FeNC have a mass fraction of Ni of 2.46 wt % and Fe of 1.96 wt %, respectively, whereas commercial Ni/C has a greater mass fraction of Ni of roughly 11.41 wt %.

Using phenolic-resin-based nanoparticles as the main carbon source may be the reason for the silica concentration found in FeNiNC, FeNC, and NiNC catalysts. The latter can also explain the ability of these catalysts to retain higher amounts of water due to the hydrophilic nature of silica, which can play a relevant role, especially under the electrolyzer mode, when it is fundamental to facilitate water molecules reaching active sites.

Furthermore, nitrogen loadings in commonly produced FeNC catalysts typically range from 1 at. % to a maximum of 10 at. %.[31] In this work, the overall amount of nitrogen over the surface of the catalysts was 5.26 at. %, 1.75 at. %, 2.28 at. %, and 0.93 at. % for FeNiNC, NiNC, FeNC, and FeNiNC/Ketjenblack, respectively. Thus, the presence of nitrogen in the

https://doi.org/10.1021/acsomega.6c07541
ACS Omega 2026, 11, 61767−61780

Downloaded from pubs.acs.org/acsodf/article-pdf/11/40/61767/6872059/acsomega.6c07541.pdf by UNIVERSIDADE DO PORTO 01100 user on 25 November 2026

FeNiNC/Ketjenblack matrix is, in fact, substantially lower, which can influence its ORR/OER activity and stability. The ORR activity of PGM-free catalysts is normally attributed to N-coordinated metal active sites, following the sequence of pyridinic nitrogen (398.6 eV) > Metal-N_x (399.7 eV) > pyrrolic N (401.0 eV) > graphitic N (403.4 eV) > oxidized N species (404.6 eV).[32] The type of nitrogen in each catalyst is revealed in Figure 4d (Deconvolution of N 1s, Figure S1), which shows an apparent strong amount of pyridinic N in the prepared PGM-free catalysts. Pyridinic nitrogen is generally considered the most active site for the ORR due to its ability to promote electron transfer and facilitate the adsorption of oxygen molecules. Also, large amounts of pyridinic nitrogen are responsible for improving the surface wettability of catalysts, which is also particularly relevant to guarantee enhanced oxygen evolution activity.[33]

The oxidation state of the species at the catalyst near-surface was evaluated using XPS. Figure 5a shows the deconvolution of the orbital Fe 2p attributed to FeNiNC and Figure 5b, Figure 5c and Figure 5d display Ni 2p deconvolution of FeNiNC, NiNC, and Ni/C, respectively. Overall, oxidized Ni and Fe structures are the prevailing species dispersed over the prepared nitrogen-doped carbon supports, thereby being able to coordinate with N; on the other hand, a stronger number of nanoparticles can be found in metallic state in the structure of the commercial Ni/C. Avoiding the formation of metallic Ni or Fe nanoparticles is essential since they are considered less active toward ORR.[34] In detail, Ni/C displayed a Ni^{2+} peak at 856.37 eV and a prominent peak ascribed to metallic Ni^0 at 854.44 eV, while those peaks appear at 856.19 and 854.15 eV for the NiNC catalyst, respectively.[35] In addition, a peak of Ni^{3+} was identified at 858.49 eV in the NiNC spectrum.

Moreover, FeNiNC revealed peaks assigned to Fe^{2+} and Fe^{3+} at 711.02 and 713.32 eV binding energies, respectively. The presence of Fe^{3+} species over the catalyst is seen as beneficial since DFT calculations have demonstrated that Fe^{3+} sites play a dominant role during OER, exhibiting suitable electrophilicity to proceed with the water oxidation reaction.[36] Fe^{2+} and Fe^{3+} peaks appear at lower binding energies of 710.23 and 711.77 eV in the FeNC results, respectively (Figure S1d). Thus, this shift in the binding energy may indicate a change in the chemical oxidation state of iron when nickel is incorporated into the structure of the FeNiNC catalyst. Furthermore, the deconvolution of the Ni 2p orbital of FeNiNC displays a Ni^{2+} peak at 855.82 eV, and no peaks are ascribed to Ni^{3+}, implying that nickel atoms spread across this catalyst have a lesser proclivity to oxidize to Ni^{3+}, thereby maintaining a lower valence.[37] Such an effect may be related to iron species on the catalyst that can stabilize nickel atoms. Particularly, it has been established that Ni^{2+} is an active species for oxygen evolution and that in FeNi catalysts, Ni^{3+} can be reduced to Ni^{2+} via H-transfer when a Fe^{2+} ion is adsorbed nearby; in this case, the overpotential toward OER significantly reduces.[38]

Figure 6 shows XRD patterns of the prepared catalysts; as all the catalysts were supported in a carbonaceous structure, each XRD pattern displays the existence of carbon lattice planes (002) and (100) at 27.9° and 43.7°, respectively, while the peak at 21.8° indicates the presence of SiO_2 within the structure of the phenolic resin-derived carbons, confirming XPS results. The carbon peak at 43.7° observed for FeNiNC, FeNC, and FeNiNC/Ketjenblack, on the other hand, may overlap with a Fe_3O_4 peak. Furthermore, the peaks assigned to FeNC pattern

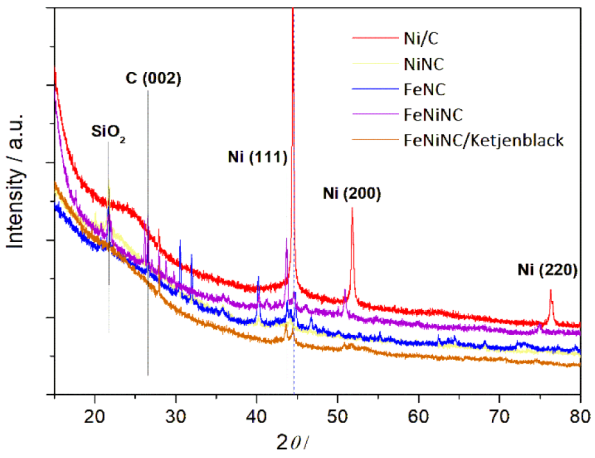

Figure 6. XRD patterns of the prepared catalysts.

at 30.6°, 31.9°, and 40.2° may also be related to iron oxide phases.[39] The typical volcano plot for OER suggests that nickel and iron oxides/hydroxides are the most active catalysts for oxygen evolution in alkaline media. Then, the presence of these species in the prepared catalysts is suggested to enhance their OER activity.[40]

Ni/C exhibits the cubic phase of Ni metal (JSPDS NO. 04−0850) attributed to the observed lattice planes (111), (200), and (220) at 44.4°, 51.9° and 76.4°, respectively.[41] The peak of Ni (111) at 44.4° is also present in the FeNiNC/Ketjenblack pattern, while it has a 0.2° positive shift in the FeNiNC pattern. The latter shows prominent peaks at 44.6° and 51.0°, which may also correspond to the (111) and (200) facets of Fe_3Ni_2 (JCPDS 65−3107), respectively.[42] Besides, the peaks at 30.0° and 75.0° can be assigned to the (220) and (533) planes of $NiFe_2O_4$, respectively. According to Li et al., the production of $NiFe_2O_4$ species may indeed be responsible for yielding larger OER activities for bimetallic structures.[43] Therefore, in this work, the incorporation of Ni and Fe atoms may ultimately lead to the formation of an intermetallic relation between Fe/Ni, which is seen as potentially beneficial to improve the intrinsic activity of the produced FeNiNC catalyst.

3.2. RDE Measurements

Rotating disk electrode (RDE) measurements were performed to assess the intrinsic activity of the prepared catalysts toward oxygen-involving reactions in 0.1 M KOH O_2-saturated electrolyte. Figure 7 shows LSV results obtained at 1600 rpm and 20 mV s^{-1} whereas Table 1 reveals the half-wave potential ($E_{1/2}$), onset potential (E_0), and Tafel slope of the prepared catalysts; it also includes the overpotential needed to provide a current density of 10 mA cm^{-2} (η_0), which is usually used to assess OER activity.

Overall, Pt/C has demonstrated improved electrochemical performance toward oxygen reduction at the beginning of life (BoL), as well as a greater diffusion-limiting current (Figure 7). Nonetheless, FeNiNC, NiNC, and FeNC catalysts demonstrated significantly enhanced mass transport while operating in electrolyzer mode, especially when compared to the standard catalysts Pt/C and IrO_2. The high surface area of the phenolic resin-derived carbon support may help in the efficient release of oxygen gas created during the oxygen evolution process, reducing the formation of gas bubbles at the electrode surface, which would further inhibit the reaction.[44] The latter explains the lower overpotentials required to achieve

Downloaded from pubs.acs.org/acsodf/article-pdf/11/40/61767/6872059/acsomega.6c07541.pdf by UNIVERSIDADE DO PORTO 01100 user on 25 November 2026

https://doi.org/10.1021/acsomega.6c07541
ACS Omega 2026, 11, 61767−61780

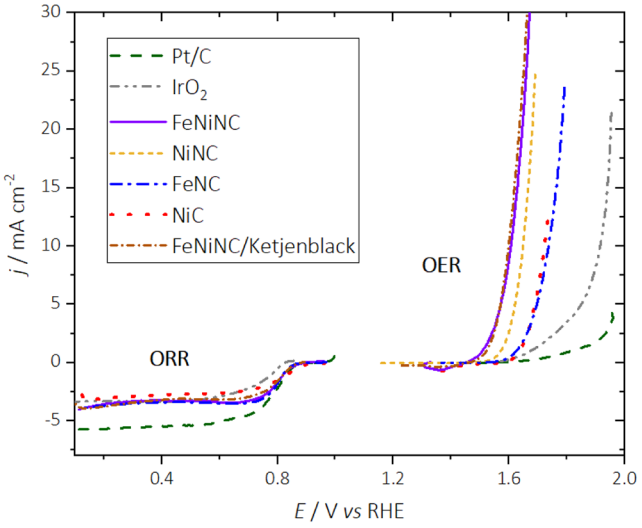

Figure 7. OER and ORR performance of the prepared catalysts, retrieved by cycling the working electrode potential between 0.05 and 2 V at 1600 rpm in 0.1 M KOH and a scan rate of 20 mV s^{-1}. Catalyst loading of 400 μg cm^{-2}.

larger current densities. On the other hand, while operating in fuel cell mode, the microporosity of the PGM-free catalysts is more likely to result in flooding, which then prevents the proper transport of gas reactants through the catalyst layer, resulting in higher mass transport overpotentials;[45] this may account for the lower current densities in the negative polarization reached by PGM-free catalysts for oxygen reduction, as seen in Figure 7.

XPS analysis (Figure 5) reveals that the newly prepared catalysts exhibit a slightly higher oxygen concentration on their surfaces compared to FeNiNC/Ketjenblack, which can help to improve their hydrophilicity/wettability. This is advantageous in the water electrolyzer (WE) operating mode. However, it can lead to mass transport overpotentials when operating in fuel cell (FC) mode.[46] Furthermore, this moderate presence of oxygenated species might be partially due to amorphous metal oxides and/or hydroxides over their surfaces, as indicated by XRD. These species are known to be particularly active for the oxygen evolution.

Interestingly, commercial Ni/C exhibits fair ORR parameters, namely an onset potential of 0.93 V and a half-wave potential of 0.73 V vs. RHE. These results are comparable to the noble Pt/C, which displays an onset potential E_0 of 0.94 V and half-wave potential of 0.73 V, and with the prepared FeNC catalyst $-E_0$ = 0.90 V and $E_{1/2}$ = 0.72 V. The prepared NiNC and FeNiNC showed slightly inferior values, displaying an E_0 of 0.86 and 0.88 V, respectively; though, such onset potentials for ORR are still equivalent to the noble catalyst IrO_2, which in turn revealed the lowest onset potential of 0.85 V.

FeNi-based catalysts displayed the earliest OER onset potential and, thereby, the lowest corresponding anodic overpotential (370−380 mV), which may result from the positive synergetic effect between iron and nickel nanoparticles. In detail, IrO_2, FeNC, NiNC, and FeNiNC reached 10 mA cm^{-2} at the potentials of 1.91, 1.74, 1.65, and 1.61 V respectively. These results are aligned with the literature; for example, Y. Chen et al. revealed similar results for FeNC catalysts decorated with $NiFe_2O_4$ while using 0.1 M KOH as a supporting electrolyte. Their $NiFe_2O_4$/FeNC catalysts revealed an overpotential of 310 mV at 10 mA cm^{-2}, which was significantly lower than that observed for RuO_2 (360 mV), $NiFe_2O_4$/Ketjenblack (380 mV), Fe_2O_3/FeNC (380 mV), and FeNC (460 mV).[39] Z. Zhang et al., prepared a supported nickel-based catalyst for OER in alkaline environment, namely $NiO/NiCo_2O_4$ which revealed an overpotential of 357 mV at 10 mA cm^{-2} and half-wave potential of 0.73 V (ORR); on the contrary, to the current work, Zhang's catalyst was assessed in a 1 M KOH supporting electrolyte, which enhances the ion conductivity of the solution and, as a result, increases the rate of oxygen evolution, masking the true influence of the catalyst structure on its final electroactivity.[46] Moreover, FeNiNC, NiNC, and FeNC exhibit OER Tafel slopes of 61 mV dec^{-1}, 60 mV $dec^{-1,}$ and 55 mV dec^{-1}, respectively. These values are comparable to those of commercial Ni/C catalysts (53 mV dec^{-1}) and remarkably lower than the benchmark IrO_2 (110 mV dec^{-1}), indicating an enhanced OER kinetics of the reported PGM-free catalysts.

The potential gap, ΔE, between the OER potential at 10 mA cm^{-2} and the half-wave potential for ORR, is a critical parameter for assessing the bifunctionality of the electrocatalysts. A lower potential gap means higher bifunctionality as the catalysts can easily switch between the two reactions closer to their thermodynamic potentials. FeNiNC displayed the lowest potential gap of 0.85 V, whereas IrO_2 revealed a ΔE of 1.19 V, and the Pt/C catalyst did not reach 10 mA cm^{-2}. A. Aijaz et al., reported a similar reversible overpotential of 0.85 V with an electrocatalyst consisting of $Co@Co_3O_4$ embedded in nitrogen-doped carbon nanotubes.[47] J. Wang et al., reported a nitrogen-doped carbon nanoshell (Fe@N−C) with a potential gap of 0.88 V[48] while, in 2017, S. Cai et al., synthesized a complex three-dimensional (3D) electrocatalyst of Co−N codoped hollow carbon sphere (HCS) which displayed a 0.856 V reversible potential.[49] Also, most of the reported catalysts are made of metal-based materials, whereas, in the present study, the overall mass fraction of metallic species on the prepared

Table 1. Electrochemical Parameters of the Prepared Catalysts toward OER/ORR—Half-Wave Potential $E_{1/2}$, Onset Potential E_0, Overpotential at 10 mA cm^{-2} and Tafel Slope, Measured in 0.1 M KOH at 25 °C

	ORR			OER		
Catalyst	$E_{1/2}$ / V	E_0 / V	Tafel Slope/mV dec^{-1}	η_0 @ 10mA cm^{-2} /mV	E_0 / V	Tafel Slope/mV dec^{-1}
FeNiNC/Ketjenblack	0.74	0.85	41	370	1.46	37
FeNiNC	0.76	0.86	118	380	1.48	61
IrO_2	0.72	0.85	14	680	1.56	110
Ni/C	0.73	0.93	61	490	1.57	53
FeNC	0.72	0.90	64	510	1.48	55
NiNC	0.74	0.88	57	420	1.51	60
Pt/C	0.73	0.94	83	-	1.54	45

https://doi.org/10.1021/acsomega.6c07541
ACS Omega 2026, 11, 61767−61780

Downloaded from pubs.acs.org/acsodf/article-pdf/11/40/61767/6872059/acsomega.6c07541.pdf by UNIVERSIDADE DO PORTO 01100 user on 25 November 2026

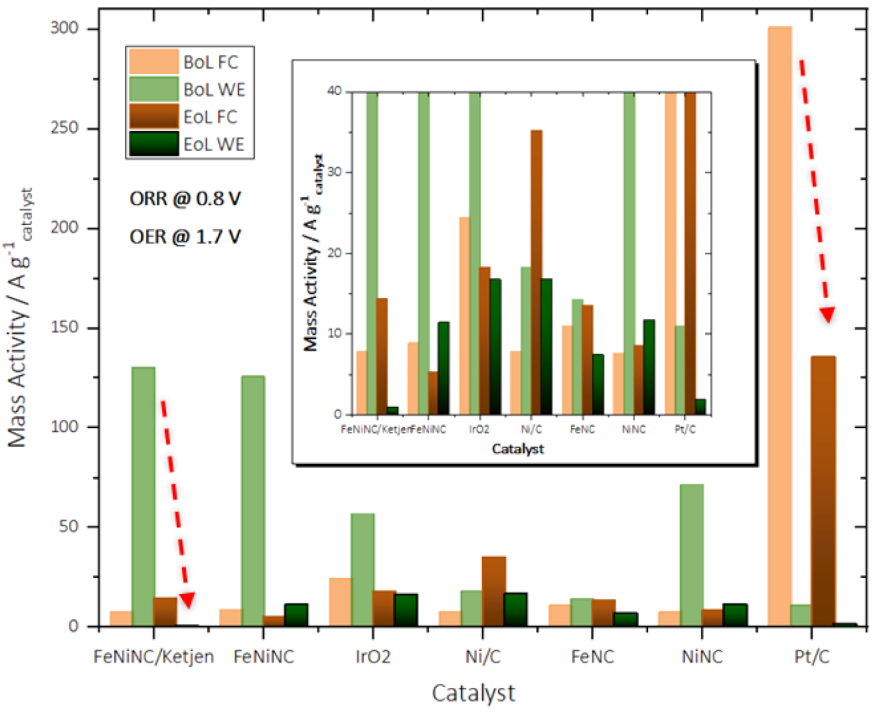

Figure 8. Mass-activity of prepared catalysts toward ORR/OER, before and after applying the stability protocol consisting of cycling the potential of the working electrode between 0.6 V and 2 V for 3000 cycles at 500 mV s^{-1}, evaluated at 0.8 V (vs RHE) and 1.7 V (vs RHE).

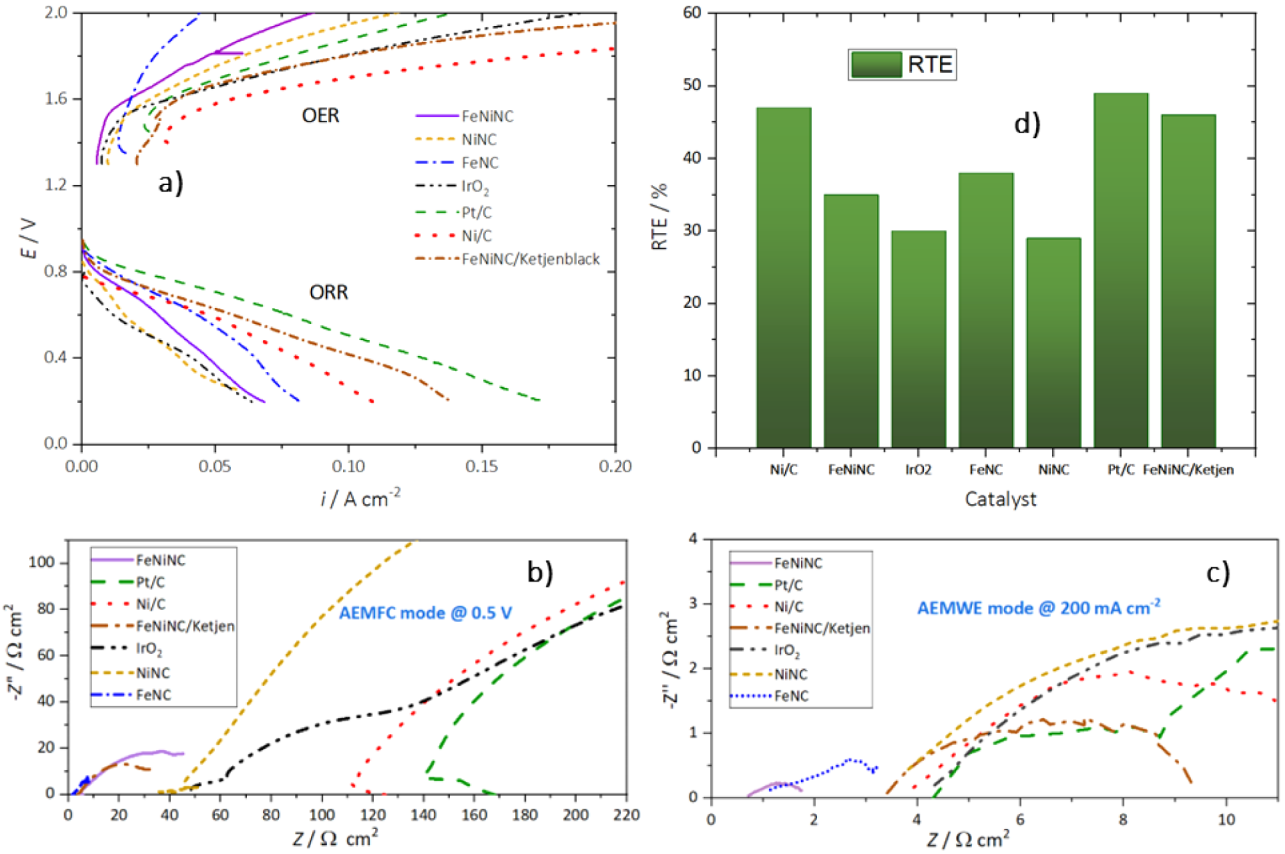

Figure 9. Polarization curves to ORR/OER of the PGM-free prepared catalysts compared with Pt/C, Ni/C, and IrO_2 catalysts, recorded at 10 mV s^{-1} (a); impedance spectra in FC mode for the oxygen electrodes in FC mode recorded at 0.5 V (b), and in WE mode recorded at 200 mA cm^{-2} (c); RTE for each catalyst, obtained using H_2:O_2 under fully humidified conditions in fuel cell mode at 1 bar and 0.5 M KOH in electrolyzer mode (d). The loading of the PGM-free catalysts is 3 mg cm^{-2} and Pt/C is 1 mg cm^{-2}.

Downloaded from pubs.acs.org/acsodf/article-pdf/11/40/61767/6872059/acsomega.6c07541.pdf by UNIVERSIDADE DO PORTO 01100 user on 25 November 2026

https://doi.org/10.1021/acsomega.6c07541
ACS Omega 2026, 11, 61767−61780

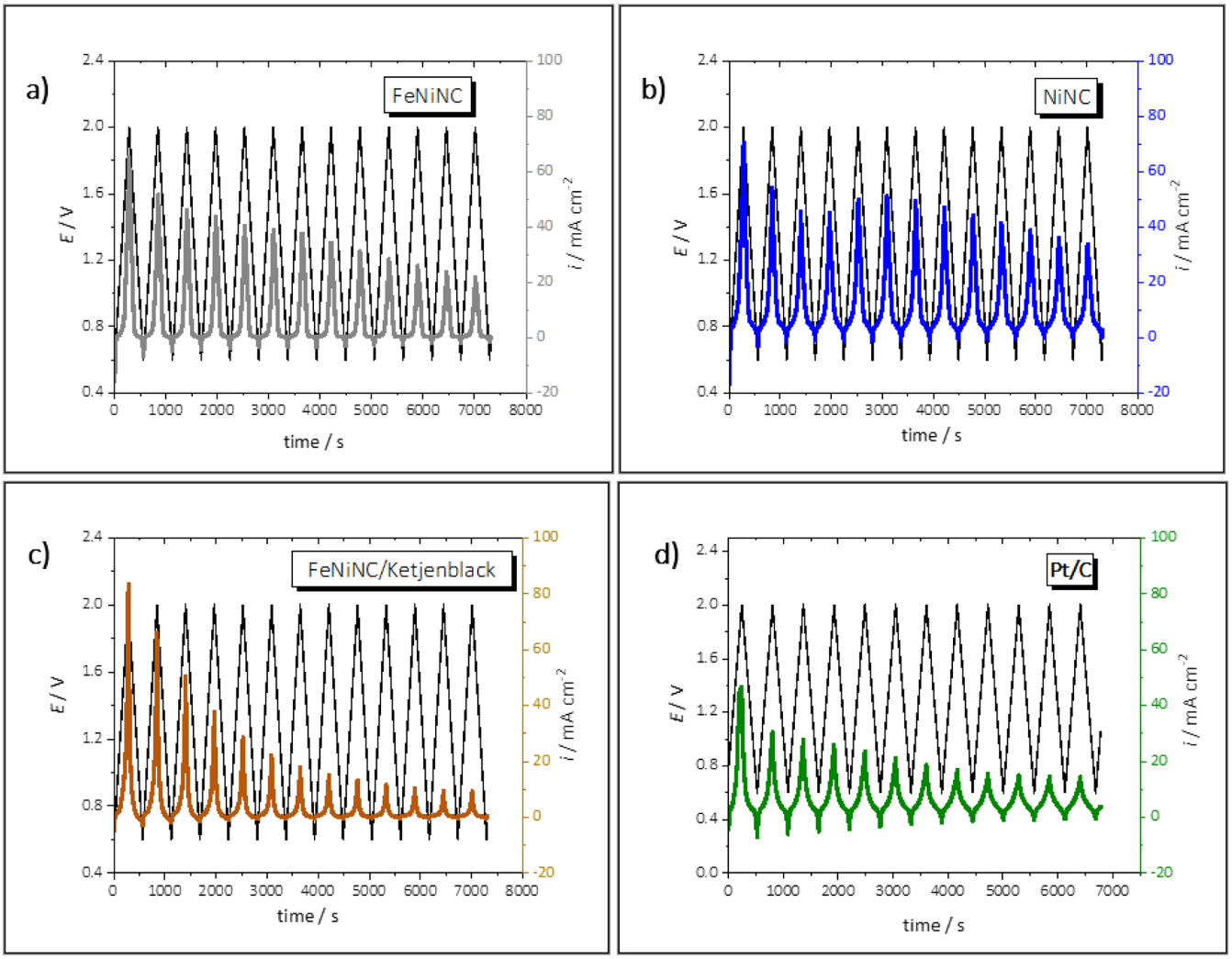

Figure 10. Performance of the UR-AEMFC during stress test using FeNiNC (**a**); NiNC (**b**); FeNiNC/Ketjenblack (**c**); and noble Pt/C (**d**), as bifunctional ORR/OER catalysts. During the stability test, the potential of the working electrode was continuously cycled between 0.5 V and 2 V for 8000 s at 5 mV s^{-1}.

PGM-free catalysts does not exceed 3%. Accelerated stress experiments (ASTs) in the RDE were used to assess the long-term stability of produced catalysts, which was then compared to the stability of benchmark noble metal catalysts. The catalysts were continuously cycled between the FC and WE operation potential ranges, namely from 0.6 to 2 V (vs RHE) for 3000 cycles at 500 mV s^{-1}. This wide potential window covers both fuel cell (lower potentials) and water electrolyzer (higher potentials) operating ranges while the fast scan rate further accelerates the stress on the catalyst.

Figure 8 summarizes the ORR/OER activity results before and after the stability test; the values were retrieved at 0.8 V vs RHE under fuel cell mode and 1.7 V vs RHE toward OER. Despite Pt/C's improved ORR activity at BoL, its performance dropped by ca. 55% after the stability test. At BoL, the prepared PGM-free catalysts demonstrated equivalent ORR activity to the benchmark Ni/C catalyst. ORR activity of FeNC, NiNC, and Ni/C at 0.8 V slightly increased after cycling the potential for 3000 cycles while FeNiNC performance decreased by 40%.

The FeNiNC catalyst exhibited exceptional OER performance at the beginning of life, achieving 125 A g^{-1} at 1.7 V, which is more than double the activity of commercial IrO_2. While FeNiNC/Ketjenblack initially showed improved OER activity, it suffered almost complete activity loss after stability testing in water electrolysis. In contrast, the prepared catalysts supported on phenolic resin-derived carbons showed overall lower performance drops during the stress test. This also confirms the assumption that the developed waste-derived supports possess a more robust carbonaceous structure, with nitrogen-doped heteroatoms providing a protective "shielding effect" against degradation.

3.3. Performance of PGM-Free Unitized Regenerative Alkaline Fuel Cells

Several authors have disclosed new PGM-free materials with the potential to be applied as bifunctional catalysts, but only a few revealed new insights to bridge the gap between material innovation and successful device integration. In this work, an innovative design employs identical components—including the single-cell structure, catalyst layer, diffusion media, and membrane —for both oxygen reduction and oxygen evolution processes.

MEAs were prepared as catalyst-coated substrates by spreading the catalyst ink over a pretreated carbon cloth without a microporous layer and with a PGM-free catalyst

Downloaded from pubs.acs.org/acsodf/article-pdf/11/40/61767/6872059/acsomega.6c07541.pdf by UNIVERSIDADE DO PORTO 01100 user on 25 November 2026

https://doi.org/10.1021/acsomega.6c07541
ACS Omega 2026, 11, 61767−61780

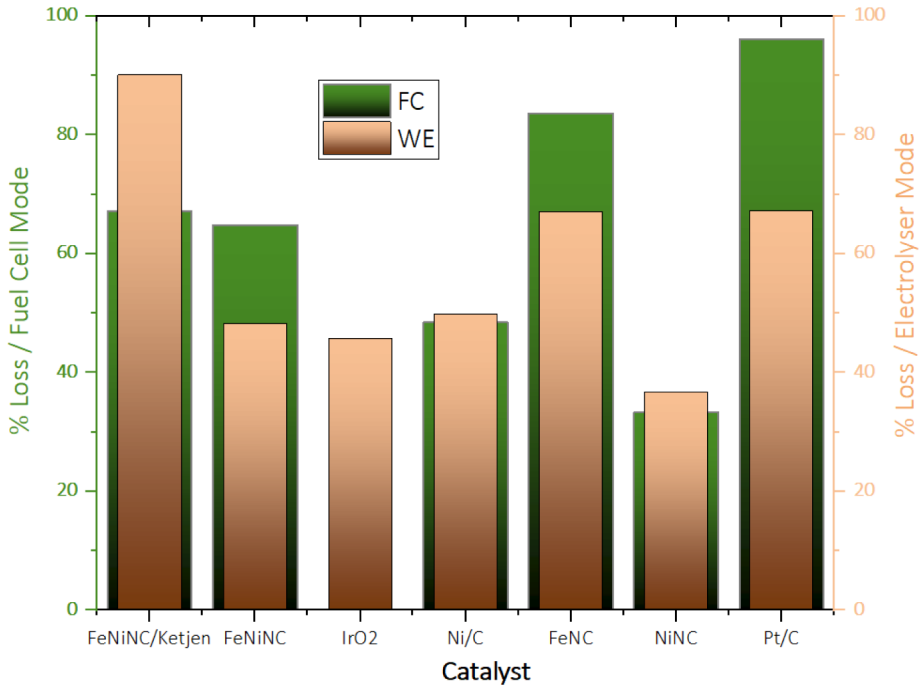

Figure 11. Performance loss of the UR-AEMFC after continuously cycling the potential between 0.5 V and 2 V at 60 °C for 8000 s at 5 mV s^{-1}.

loading of 3 mg cm^{-2}. Carbon cloths were used not only because they are a significantly less expensive alternative to commonly used bulk titanium porous transport layers, but also because preliminary experimental findings on the use of state-of-the-art carbon papers have clearly indicated that carbon corrosion on the microporous layer side of the gas diffusion layer (GDL) is a primary cause of URFC performance degradation. While the impact of carbon corrosion on electrical resistance is minimal, the voids formed at the interface between the GDL and catalyst-coated membranes are not trivial and can directly influence the water transfer capacity; therefore, both ohmic and mass transfer impedances increase substantially.[50] UR-AEMFC tests were then conducted using the prepared PGM-free catalysts, and Pt/C, IrO_2, and Ni/C as benchmark catalyst layers. The summary of the cell performance is detailed in Figure 9a.

FeNC, NiNC, FeNiNC and FeNiNC/Ketjenblack catalyst layers were tested by subjecting the cell to a constant flow of H_2/O_2 under fully humidified conditions and revealed a peak power density in fuel cell mode of 27.70, 14.79, 19.35, and 42.05 mW cm^{-2}, respectively. For comparison, commercial catalysts exhibited peak power densities of 52.01 mW cm^{-2} (Pt/C), 32.83 mW cm^{-2} (Ni/C), and 16.60 mW cm^{-2} (IrO_2) (Figure S2a). In electrolyzer mode, while running a supporting electrolyte consisting of 0.5 M KOH through the URFC system, FeNiNC/Ketjenblack reached demonstrated superior performance of 2.64 W cm^{-2} at 1.10 A cm^{-2} (Figure S2b) , followed by Ni/C and IrO_2 with 1.43 W cm^{-2} at 0.58 A cm^{-2}, and 1.02 W cm^{-2} at 0.40 A cm^{-2}, respectively.

Still, the prepared PGM-free catalysts have an overall <3 wt % of iron and/or nickel nanoparticles supported over the carbon matrix, which means that the amount of metal is extremely inferior compared to the 40 wt % Pt/C used for comparison. Additionally, the commercial Ni/C catalyst has ca. 10 times more nickel than the prepared FeNiNC and NiNC, according to the ICP results. Therefore, these catalysts achieve competitive results with significantly lower metal contents, indicating higher catalytic efficiency per unit mass of metal.

The electrochemical impedance spectroscopy (EIS) spectra recorded at 0.5 V in FC and 200 mA cm^{-2} in WE mode are represented in Figure 9b and Figure 9c, respectively. At 0.5 V, the EIS spectra in FC mode show that all Fe-based oxygen electrodes have the lowest ohmic resistances (R_{ohm}). Also, R_{ohm} is approximately 800 mΩ cm^2 in WE mode for both FeNiNC and FeNC, compared to >3 Ω cm^2 for the other metal catalysts. As a result, the total resistance (R_{total}) is less than 1 Ω cm^2 for FeNiNC and FeNC, compared to greater than 6 Ω cm^2 for Pt/C and IrO_2. These results suggest that incorporating Fe into the Ni matrix enhances electrical conductivity across the electrode. Furthermore, dispersing metallic nanoparticles across the produced N-doped carbon generally reduced resistivity across the oxygen-electrode catalyst layer.

The round-trip efficiency of the UR-AEMFCs was estimated by dividing the generated voltage in the FC mode by the consumed voltage in the WE mode, and both values were assessed at 30 mA cm^{-2}(Figure 9d). NiNC has an RTE of 29%, similar to the commercial IrO_2 catalyst, which has an overall efficiency of 30%. While FeNC and FeNiNC catalysts unveiled highly interesting efficiencies of 38% and 35%, respectively, FeNiNC/Ketjenblack showed an impressive RTE of 46%, similar to the performance achieved by commercial Ni/C and Pt/C, which reached 47% and 49%, respectively.

On the other hand, the stability of the prepared catalyst layers was assessed by cycling the cell continuously between FC and WE modes, particularly between 0.6 and 2 V at 5 mV s^{-1} for 8000 s; the results are shown in Figure 10 (polarization curves at EoL are represented in Figure S3). The prepared FeNiNC and NiNC catalysts (Figure 10a and Figure 10b) display a great trade-off between round-trip efficiency and stability when compared to FeNiNC/Ketjenblack or even Pt/C catalysts, which in turn were fully deactivated after the stress testing (Figure 10c and Figure 10d). The Pt/C catalyst layer

https://doi.org/10.1021/acsomega.6c07541
ACS Omega 2026, 11, 61767−61780

Downloaded from pubs.acs.org/acsodf/article-pdf/11/40/61767/6872059/acsomega.6c07541.pdf by UNIVERSIDADE DO PORTO 01100 user on 25 November 2026

suffered severe performance loss (Figure 10d0 which is reflected in a loss of performance at 0.5 V of 96.13% and 67.28% at 2.0 V (Figure 11). After being exposed to the stress test, IrO_2 was also completely deactivated, and FeNC—despite having shown a good RTE at BoL—revealed strong losses of 83.64% at 0.5 V and 67.04% at 2.0 V (Figure S4). Overall, NiNC has the highest stability by losing only 33.33% in fuel cell mode and 36.64% in electrolyzer mode (Figure 11).

The higher overall resistances observed for the Ketjenblack-based FeNiNC catalyst, obtained from the EIS spectra at EoL (Figure S5), confirm further its superior degradation and, on the other hand, the higher stability of the prepared phenolic resin-derived N-doped carbon supports. This is especially noticeable while operating in electrolyzer mode (performance losses considered at 2.0 V). These results are consistent with XPS spectra, which demonstrated a higher concentration of heteroatoms (N) in the structure of phenolic resin-derived carbons, typically related to a higher stability.[51] Besides, the manufactured H_3PO_4-activated carbons revealed the presence of SiO_2 in their composition; silica is a corrosion-resistant metal oxide, recently being studied as an interesting solution to improve the stability of ORR/OER catalysts.[52]

The ability of the proposed unitized regenerative fuel cells to operate efficiently can also be assessed by comparing their performance to other reported systems. For instance, N. Hassan et al. employed 2.0 mg cm^{-2} $NiCoO_x$ on the oxygen electrode, achieving a RTE of 48%. However, it is worth noting that these authors incorporated 0.5 mg cm^{-2} Pt black alongside the non-noble catalyst, potentially elevating their bifunctional performance.[53] J. W. Desmond Ng et al., prepared gas diffusion electrodes with higher loadings, namely 6 mg cm^{-2} of Ni/C for the H_2 electrode and 4 mg cm^{-2} (5:1 MnOx/GC:Ni/C by mass) for the O_2 electrode, with the results revealing an efficiency of 40% at 10 mA cm^{-2}.[54] On the other hand, C.A. Campos-Roldán et al. unveiled a system consisting of oxygen electrodes made of NiFeOx−CoNy/NCNH. The system showed a round-trip efficiency of 44.76%.[55] Nonetheless, the utilized catalyst has a higher nominal mass fraction of metal − 50% − and the cell was tested under 3 M KOH.

Future research must prevent catalyst deactivation, especially focusing on characterizing the prepared catalysts to deeply understand the reaction mechanisms and prevailing degradation routes. In addition, bridging the lab-to-industry gap is vital for improving performance, scalability, and cost-effectiveness; thus, optimizing catalyst layer preparation and reducing PGM-free loadings are key factors for future advancements.

4. CONCLUSIONS

Low-cost FeNiNC-, NiNC-, and FeNC-based bifunctional catalysts were developed for UR-AEMFC, with excellent activities and stabilities per mass of metal, outperforming benchmark PGM catalysts for operation in an alkaline environment.

All of the prepared catalysts were supported on waste-derived N-doped carbon supports and unveiled significant stability; indeed, using circular economy approaches is essential for increasing the sustainability of new materials manufacturing. Among them, the FeNi catalyst exhibited the most favorable bifunctional behavior, indicating that the combination of Fe and Ni can provide complementary catalytic functionalities for ORR and OER.

Thus, this work presents a novel catalyst, with favorable activity and stability, even under ultralow metal loading. Moreover, it provides crucial insights into the development of sustainable non-noble catalysts for URFC systems, which may be a promising approach to assist in the fluctuations and intermittency of renewable energy sources by balancing the electrical grid at a low cost.

■ ASSOCIATED CONTENT

Supporting Information

The Supporting Information is available free of charge at https://pubs.acs.org/doi/10.1021/acsomega.6c07541.

Table S1 − BET and TEM results; Figure S1 − XPS of prepared catalysts; Figure S2 − Peak power density; Figure S3 − Polarization curves; Figure S4 − Operation of UR-AEMFC; Figure S5 − Nyquist plots (PDF)

■ AUTHOR INFORMATION

Corresponding Author

Adélio Mendes − *LEPABE − Laboratory for Process Engineering, Environment, Biotechnology and Energy, ALiCE − Associate Laboratory in Chemical Engineering, Faculty of Engineering, University of Porto, Porto 4200-465, Portugal;* orcid.org/0000-0003-2472-3265; Email: mendes@fe.up.pt

Authors

Eva Sousa − *LEPABE − Laboratory for Process Engineering, Environment, Biotechnology and Energy, ALiCE − Associate Laboratory in Chemical Engineering, Faculty of Engineering, University of Porto, Porto 4200-465, Portugal*

Sofia Delgado − *LEPABE − Laboratory for Process Engineering, Environment, Biotechnology and Energy, ALiCE − Associate Laboratory in Chemical Engineering, Faculty of Engineering, University of Porto, Porto 4200-465, Portugal*

Fátima Santos − *LEPABE − Laboratory for Process Engineering, Environment, Biotechnology and Energy, ALiCE − Associate Laboratory in Chemical Engineering, Faculty of Engineering, University of Porto, Porto 4200-465, Portugal;* orcid.org/0000-0002-9029-4107

Complete contact information is available at: https://pubs.acs.org/10.1021/acsomega.6c07541

Author Contributions

◆E.S. and S.D. contributed equally for this work. E.S. − Conceptualization, Methodology, Investigation, Writing − original draft; S.D. − Conceptualization, Methodology, Investigation, Writing − review and editing. F.S. − Writing − review and editing. A.M. − Conceptualization, Supervision, Project administration, Funding Acquisition, Writing − review and editing.

Notes

The authors declare no competing financial interest.

■ ACKNOWLEDGMENTS

Eva Sousa and Sofia Delgado are grateful to the Portuguese Foundation for Science and Technology (FCT) for the doctoral grants (references SFRH/BD/145412/2019, SFRH/BD/144338/201, respectively). F.S. acknowledges the FCT for her research grant reference 2023.07366.CEECIND/CP2834/CT0012 (10.54499/2023.07366.CEECIND/CP2834/CT0012). The research leading to these results also received

Downloaded from pubs.acs.org/acsodf/article-pdf/11/40/61767/6872059/acsomega.6c07541.pdf by UNIVERSIDADE DO PORTO 01100 user on 25 November 2026

funding from (i) project Baterias 2030, with the reference POCI-01-0247-FEDER-046109, cofunded by Operational Programme for Competitiveness and Internationalisation (COMPETE 2020), under the Portugal 2020 Partnership Agreement, through the European Regional Development Fund (ERDF); and (ii) national funds through FCT/MECI: LEPABE, UID/00511/2025 (10.54499/UID/00511/2025) and UID/PRR/00511/2025 (10.54499/UID/PRR/00511/2025) and ALiCE, LA/P/0045/2020 (10.54499/LA/P/0045/2020).

REFERENCES

(1) Liu, X.; Li, W.; Guo, X.; Su, B.; Guo, S.; Jing, Y.; Zhang, X. Advancements in Energy-Storage Technologies: A Review of Current Developments and Applications. *Sustainability* **2025**, *17*, 8316.
(2) Degen, F.; Winter, M.; Bendig, D.; Tübke, J. Energy consumption of current and future production of lithium-ion and post lithium-ion battery cells. *Nat. Energy* **2023**, *8*, 1284−1295.
(3) Vincent, I.; Perez, N. A.; Minudri, D.; Fernandez-Carretero, F.; Gesalaga, E. F.; Garcia-Luis, A.; Kim, H.-M. A roadmap to a low-cost anion exchange membrane Unitized regenerative fuel cell. *Sustainable Energy Fuels* **2025**, *9* (21), 5772−5790.
(4) Mladenović, D.; Mladenović, A.; Santos, D. M. F.; Yurtcan, A. B.; Miljanić, Š.; Mentus, S.; Šljukić, B. Transition metal oxides for bifunctional ORR/OER electrocatalysis in unitized regenerative fuel cells. *J. Electroanal. Chem.* **2023**, *946*, 117709.
(5) Vincent, I.; Lee, E. C.; Kim, H. M. Solutions to the water flooding problem for unitized regenerative fuel cells: status and perspectives. *RSC Adv.* **2020**, *10*, 16844−16860.
(6) Wang, Y.; Leung, D. Y. C.; Xuan, J.; Wang, H. A review on unitized regenerative fuel cell technologies, part-A: Unitized regenerative proton exchange membrane fuel cells. *Renewable Sustainable Energy Rev.* **2016**, *65*, 961−977.
(7) Lim, A.; Kim, J.; Lee, H. J.; Kim, H. J.; Yoo, S. J.; Jang, J. H.; Young Park, H.; Sung, Y. E.; Park, H. S. Low-loading IrO2 supported on Pt for catalysis of PEM water electrolysis and regenerative fuel cells. *Appl. Catal., B* **2020**, *272*, 118955.
(8) Salonen, L. M.; Petrovykh, D. Y.; Kolen'ko, Y. V. Sustainable catalysts for water electrolysis: Selected strategies for reduction and replacement of platinum-group metals. *Mater. Today. Sustainable* **2021**, *11-12*, 100060.
(9) Lewicka, E.; Guzik, K.; Galos, K. On the possibilities of critical raw materials production from the eu's primary sources. *Resources* **2021**, *10* (5), 50.
(10) Peng, H.; Li, Q.; Hu, M.; Xiao, L.; Lu, J.; Zhuang, L. Alkaline polymer electrolyte fuel cells stably working at 80 °C. *J. Power Sources* **2018**, *390*, 165−167.
(11) Kaczur, J. J.; Yang, H.; Liu, Z.; Sajjad, S. D.; Masel, R. I. Carbon dioxide and water electrolysis using new alkaline stable anion membranes. *Front. Chem.* **2018**, *6*, 263.
(12) Pico, P. P. M.; Montero, J.; Tsurumaki, A.; Passerini, S.; Navarra, M. A. Bifunctional PGM-free electrocatalysts for seawater batteries. *Sustainable Energy Fuels* **2026**, *10* (1), 227−235.
(13) Kelly, S. R.; Kirk, C.; Chan, K.; Nørskov, J. K. Electric field effects in oxygen reduction kinetics: rationalizing ph dependence at the pt(111), au(111), and au(100) electrodes. *J. Phys. Chem. C* **2020**, *124* (27), 14581−14591.
(14) Tang, J.; Su, C.; Zhong, Y.; Shao, Z. Oxide-based precious metal-free electrocatalysts for anion exchange membrane fuel cells: From material design to cell applications. *J. Mater. Chem. A* **2021**, *9*, 3151−3179.
(15) Li, W.; Jin, R.; Zhang, M.; Mao, X.; Xie, F.; Chen, J.; Wang, N.; Jin, Y.; Lu, Y.; Meng, H. Electrochemical oxidation-driven synthesis of Fe-Incorporated $Ni(OH)_2$/NiOOH for enhanced alkaline oxygen evolution catalysis. *Mater. Lett.* **2025**, *400*, 139145.
(16) Zhao, J.; Zhang, J. J.; Li, Z. Y.; Bu, X. H. Recent Progress on NiFe-Based Electrocatalysts for the Oxygen Evolution Reaction. *Small* **2020**, *16* (51), 2003916.
(17) Gallenkamp, C.; Kramm, U. I.; Proppe, J.; Krewald, V. Calibration of computational Mössbauer spectroscopy to unravel active sites in FeNC catalysts for the oxygen reduction reaction. *Int. J. Quantum Chem.* **2021**, *121* (3), No. e26394.
(18) Zheng, Y.; Chen, S.; Yu, X.; Li, K.; Ni, X.; Ye, L. Nitrogen-doped carbon spheres with precisely-constructed pyridinic-N active sites for efficient oxygen reduction. *Appl. Surf. Sci.* **2022**, *598*, 153786.
(19) Lin, Y.; Liu, Z.; Yu, L.; Zhang, G. R.; Tan, H.; Wu, K. H.; Song, F.; Mechler, A. K.; Schleker, P. P. M.; Lu, Q.; Zhang, B.; Heumann, S. Overall Oxygen Electrocatalysis on Nitrogen-Modified Carbon Catalysts: Identification of Active Sites and In Situ Observation of Reactive Intermediates. *Angew. Chem., Int. Ed.* **2021**, *60*, 3299−3306.
(20) Wang, Q.; Shang, L.; Sun-Waterhouse, D.; Zhang, T.; Waterhouse, G. Engineering local coordination environments and site densities for high-performance Fe-N-C oxygen reduction reaction electrocatalysis. *SmartMat* **2021**, *2*, 154−175.
(21) Garche, J.; Smolinka, T.; Navarra, M. A.; Panero, S.; Scrosati, B.Regenerative fuel cells*Electrochemical Power Sources: Fundamentals, Systems, and Applications*Elsevier2022365−406
(22) Chen, W.; Meng, K.; Zhou, H.; Zhang, N.; Deng, Q.; Chen, K.; Chen, B. Mass transfer and round-trip efficiency evaluation of unitized regeneration proton exchange membrane fuel cell during bi-directional mode switching cycle. *Appl. Energy* **2024**, *374*, 124076.
(23) Hu, Y.; Deng, J.; Ren, P.; Yang, F.; Zhang, L.; Li, Y. Reconciling opposing demands on unitized regenerative fuel cells: From bifunctional materials and operational management to durability. *Chem. Eng. Process.* **2026**, *225*, 110809.
(24) Yang, H.; Chen, P.; Chen, W.; Li, K.; Xia, M.; Xiao, H.; Chen, X.; Chen, Y.; Wang, X.; Chen, H. Insight into the formation mechanism of N, P co-doped mesoporous biochar from H3PO4activation and NH3 modification of biomass. *Fuel Process. Technol.* **2022**, *230*, 107215.
(25) Sengupta, I.; Chakraborty, S.; Talukdar, M.; Pal, S. K.; Chakraborty, S. Thermal reduction of graphene oxide: How temperature influences purity. *J. Mater. Res.* **2018**, *33*, 4113−4122.
(26) Hintsho, N.; Shaikjee, A.; Tripathi, P. K.; Franklyn, P.; Durbach, S. The effect of CO2 on the CVD synthesis of carbon nanomaterials using fly ash as a catalyst. *RSC Adv.* **2015**, *5*, 53776−53781.
(27) Sing, K. S. W. Physisorption of Nitrogen by Porous Materials. *J. Porous Mater.* **1995**, *2*, 5−8.
(28) Xia, D.; Yu, C.; Zhao, Y.; Wei, Y.; Wu, H.; Kang, Y.; Li, J.; Gan, L.; Kang, F. Degradation and regeneration of Fe-Nxactive sites for the oxygen reduction reaction: The role of surface oxidation, Fe demetallation and local carbon microporosity. *Chem. Sci.* **2021**, *12*, 11576−11584.
(29) Fletcher, A. J.; Uygur, Y.; Mark Thomas, K. Role of surface functional groups in the adsorption kinetics of water vapor on microporous activated carbons. *J. Phys. Chem. C* **2007**, *111* (23), 8349−8359.
(30) Ganesan, S.; Leonard, N.; Barton, S. C. Impact of transition metal on nitrogen retention and activity of iron-nitrogen-carbon oxygen reduction catalysts. *Phys. Chem. Chem. Phys.* **2014**, *16*, 4576−4585.
(31) Li, B.; Jervis, R. Advancing Fe−N−C catalysts: synthesis strategies and performance enhancements for fuel cell applications. *Energy Adv.* **2025**, *4*, 1412−1425.
(32) Zhang, J.; Sun, Y.; Zhu, J.; Kou, Z.; Hu, P.; Liu, L.; Li, S.; Mu, S.; Huang, Y. Defect and pyridinic nitrogen engineering of carbon-based metal-free nanomaterial toward oxygen reduction. *Nano Energy* **2018**, *52*, 307−314.
(33) Chen, D.; Zhu, J.; Mu, X.; Cheng, R.; Li, W.; Liu, S.; Pu, Z.; Lin, C.; Mu, S. Nitrogen-Doped carbon coupled FeNi3 intermetallic compound as advanced bifunctional electrocatalyst for OER, ORR and zn-air batteries. *Appl. Catal., B* **2020**, *268*, 118729.
(34) Zhou, Y.; Al-Zoubi, T.; Ma, Y.; Hsiao, H. W.; Zhang, C.; Sun, C.; Zuo, J. M.; Yang, H. Boosting the activity of non-platinum group metal electrocatalyst for the reduction of oxygen via dual-ligated

Downloaded from pubs.acs.org/acsodf/article-pdf/11/40/61767/6872059/acsomega.6c07541.pdf by UNIVERSIDADE DO PORTO 01100 user on 25 November 2026

https://doi.org/10.1021/acsomega.6c07541
ACS Omega 2026, 11, 61767−61780

atomically dispersed precursors immobilized on carbon supports. *Nano Energy* **2021**, *90*, 106547.
(35) Gu, X.; Liu, Z.; Li, M.; Tian, J.; Feng, L. Surface structure regulation and evaluation of FeNi-based nanoparticles for oxygen evolution reaction. *Appl. Catal., B* **2021**, *297*, 120462.
(36) Friebel, D.; Louie, M. W.; Bajdich, M.; Sanwald, K. E.; Cai, Y.; Wise, A. M.; Cheng, M. J.; Sokaras, D.; Weng, T. C.; Alonso-Mori, R.; Davis, R. C.; Bargar, J. R.; Nørskov, J. K.; Nilsson, A.; Bell, A. T. Identification of highly active Fe sites in (Ni,Fe)OOH for electrocatalytic water splitting. *J. Am. Chem. Soc.* **2015**, *137*, 1305−1313.
(37) Ma, M.; Kumar, A.; Wang, D.; Wang, Y.; Jia, Y.; Zhang, Y.; Zhang, G.; Yan, Z.; Sun, X. Boosting the bifunctional oxygen electrocatalytic performance of atomically dispersed Fe site via atomic Ni neighboring. *Appl. Catal., B* **2020**, *274*, 119091.
(38) Chen, D.; Perilli, D.; Dronskowski, R.; Selloni, A.; Valentin, C. D. Enhanced oxygen evolution on NiOOH through Fe-promoted transformation of β to γ phase. *Acta Mater.* **2025**, *299*, 121434.
(39) Chen, Y.; Li, G.; Hong, L.; Wang, Y.; Wang, N.; Liu, Z.; Lin, W.-F.; Shi, Z. FeNC Catalysts Decorated with NiFe2O4 to Enhance Bifunctional Activity for Zn−Air Batteries. *ACS Appl. Energy Mater.* **2023**, *6*, 6357−6369.
(40) Jafari, F.; Najafpour, M. M. Iron−Nickel Based Catalysts for Oxygen-Evolution Reaction: Mechanism, Stability, and Potential-Dependent Role of Iron. *Inorg. Chem.* **2025**, *64* (46), 22742−22757.
(41) Fan, L.; Liu, P. F.; Yan, X.; Gu, L.; Yang, Z. Z.; Yang, H. G.; Qiu, S.; Yao, X. Atomically isolated nickel species anchored on graphitized carbon for efficient hydrogen evolution electrocatalysis. *Nat. Commun.* **2016**, *7*, 10667.
(42) Kim, M. J.; Shim, J.; Lee, K. S.; Sung, Y. E. Nonprecious Metal Bifunctional Catalysts for Oxygen Electrocatalysis Using a Metal-Organic Framework. *Bull. Korean Chem. Soc.* **2021**, *42*, 919−924.
(43) Li, Y. F.; Selloni, A. Mechanism and activity of water oxidation on selected surfaces of pure and Fe-Doped NiOx. *ACS Catal.* **2024**, *4* (4), 1148−1153.
(44) Lv, H.; Chen, J.; Zhou, W.; Shen, X.; Zhang, C. Mechanism analyses and optimization strategies for performance improvement in low-temperature water electrolysis systems via the perspective of mass transfer: A review. *Renewable Sustainable Energy Rev.* **2023**, *183*, 113394.
(45) Yang, L.; Larouche, N.; Chenitz, R.; Zhang, G.; Lefèvre, M.; Dodelet, J. P. Activity, Performance, and Durability for the Reduction of Oxygen in PEM Fuel Cells, of Fe/N/C Electrocatalysts Obtained from the Pyrolysis of Metal-Organic-Framework and Iron Porphyrin Precursors. *Electrochim. Acta* **2015**, *159*, 184−197.
(46) Zhang, Z.; Liang, X.; Li, J.; Qian, J.; Liu, Y.; Yang, S.; Wang, Y.; Gao, D.; Xue, D. Interfacial Engineering of NiO/NiCo2O4 Porous Nanofibers as Efficient Bifunctional Catalysts for Rechargeable Zinc-Air Batteries. *ACS Appl. Mater. Interfaces* **2020**, *12*, 21661−21669.
(47) Aijaz, A.; Masa, J.; Rösler, C.; Xia, W.; Weide, P.; Botz, A. J. R.; Fischer, R. A.; Schuhmann, W.; Muhler, M. Bifunktionale Sauerstoffelektroden durch Einbettung von Co@Co3O4-Nanopartikeln in CNT-gekoppelte Stickstoff-dotierte Kohlenstoffpolyeder. *Angew. Chem., Int. Ed.* **2016**, *128*, 4155−4160.
(48) Wang, J.; Wu, H.; Gao, D.; Miao, S.; Wang, G.; Bao, X. High-density iron nanoparticles encapsulated within nitrogen-doped carbon nanoshell as efficient oxygen electrocatalyst for zinc-air battery. *Nano Energy* **2015**, *13*, 387−396.
(49) Cai, S.; Meng, Z.; Tang, H.; Wang, Y.; Tsiakaras, P. 3D Co-N-doped hollow carbon spheres as excellent bifunctional electrocatalysts for oxygen reduction reaction and oxygen evolution reaction. *Appl. Catal., B* **2017**, *217*, 477−484.
(50) Li, P.; Qiu, D.; Peng, L.; Shen, S.; Lai, X. Analysis of degradation mechanism in unitized regenerative fuel cell under the cyclic operation. *Energy Convers. Manage.* **2022**, *254*, 115210.
(51) Xu, R.; Sun, N.; Zhou, H.; Chang, X.; Soomro, R. A.; Xu, B. Hard carbon anodes derived from phenolic resin/sucrose cross-linking network for high-performance sodium-ion batteries. *Battery Energy* **2023**, *2* (2), 20220054.
(52) Zeng, X.; Zhang, H.; Zhang, X.; Zhang, Q.; Chen, Y.; Yu, R.; Moskovits, M. Coupling of ultrasmall and small CoxP nanoparticles confined in porous SiO2 matrix for a robust oxygen evolution reaction. *Nano Mater. Sci.* **2022**, *4*, 393−399.
(53) Hassan, N. U.; Ganesan, P.; Lando, A. A.; Mustain, W. E.; Colón-Mercado, H. R. Stable, high-performing bifunctional electrodes for anion exchange membrane-based unitized regenerative fuel cells. *J. Power Sources* **2022**, *541*, 231599.
(54) Desmond Ng, J. W.; Gorlin, Y.; Hatsukade, T.; Jaramillo, T. F. A precious-metal-free regenerative fuel cell for storing renewable electricity. *Adv. Energy Mater.* **2013**, *3*, 1545−1550.
(55) Campos-Roldán, C. A.; Zhong, H.; Unni, S. M.; González-Huerta, R. D. G.; Feng, Y.; Alonso-Vante, N. Unitized Regenerative Alkaline Microfluidic Cell Based on Platinum Group Metal-Free Electrode Materials. *ACS Appl. Energy Mater.* **2020**, *3*, 7397−7403.

Downloaded from pubs.acs.org/acsodf/article-pdf/11/40/61767/6872059/acsomega.6c07541.pdf by UNIVERSIDADE DO PORTO 01100 user on 25 November 2026

https://doi.org/10.1021/acsomega.6c07541
ACS Omega 2026, 11, 61767−61780